PHYSICAL REVIEW B VOLUME 43, NUMBER 16 1 JUNE 1991

Magnetic excitations in the heavy-fermion superconductor URu_2Si_2

C. Broholm*
Risø National Laboratory, DK-4000 Roskilde, Denmark
and AT&T Bell Laboratories, Murray Hill, New Jersey 07974

H. Lin
Atomic Energy of Canada Ltd., Chalk River Laboratories, Chalk River, Ontario, K0J 1J0, Canada
and Department of Physics, McMaster University, Hamilton, Ontario, L8S 4M1, Canada

P. T. Matthews
Department of Physics, Queen's University, Kingston, Ontario, K7L 3N6, Canada

T. E. Mason†
Department of Physics, McMaster University, Hamilton, Ontario, L8S 4M1, Canada

W. J. L. Buyers
Atomic Energy of Canada Ltd., Chalk River Laboratories, Chalk River, Ontario, K0J 1J0, Canada

M. F. Collins
Department of Physics, McMaster University, Hamilton, Ontario, L8S 4M1, Canada

A. A. Menovsky
Natuurkundig Laboratorium Der Universiteit van Amsterdam, NL-1018XE Amsterdam, The Netherlands
and Kammerlingh Onnes Laboratorium, Rijksuniversiteit te Leiden, NL-2300RA Leiden, The Netherlands

J. A. Mydosh
Kammerlingh Onnes Laboratorium, Rijksuniversiteit te Leiden, NL-2300RA Leiden, The Netherlands

J. K. Kjems
Risø National Laboratory, DK-4000 Roskilde, Denmark

(Received 26 March 1990; revised manuscript received 19 December 1990)

Antiferromagnetic order and fluctuations in the heavy-fermion superconductor URu_2Si_2 have been studied by magnetic neutron scattering. Below $T_N = 17.5$ K, URu_2Si_2 is a type-I antiferromagnet with an anomalously small ordered moment of $(0.04\pm0.01)\mu_B$ polarized along the tetragonal c axis. Dispersive resonant excitations exist in the ordered state with a zone-center gap of 0.43 THz. The excitations are polarized along the ordered moment and have a large dipolar matrix element, which suggests that they are coupled transitions between singlet crystal-field-like states. For energy transfer above 3 THz, peaks have not been identified in the magnetic excitation spectra, but instead a continuous spectrum of scattering peaked around the ordering wave vector indicates the presence of overdamped antiferromagnetically correlated spin fluctuations. Upon heating above T_N, the resonant excitations abruptly become heavily damped but the magnetic scattering at higher energies does not change at T_N. Instead, the disappearance of the antiferromagnetic modulation of the higher-energy scattering coincides with the maximum in the resistivity of URu_2Si_2.

I. INTRODUCTION

Although URu_2Si_2 is generally considered a heavy-fermion system, some of its bulk properties$^{1-7}$ are in fact markedly different from other uranium-based heavy-fermion systems. It has a large electronic specific heat, which is approximately linear in T just above $T_N = 17.5$ K and which corresponds to^1 $\gamma = 180$ mJ/(mol K^2). A little higher above T_N, at about 30 K, there is a maximum in the electronic specific heat,^{3} which is reminiscent of a Schottky anomaly, a signature of conserved local moments in an anisotropic environment well known from rare-earth magnetism.^{8,9} Below T_N the heat capacity, apart from an exponential term which shows the presence of a gapped spectrum, has a linear term^1 $\gamma \sim 50$ mJ/(mol K^2). This is certainly much larger than that of a normal metal, but nearly an order of magnetic smaller than electronic specific-heat coefficients in other heavy-fermion systems. The bulk susceptibility of URu_2Si_2 (Refs. 1–3) shows not only features of crystal-field magnetism, a Schottky anomaly at about 50 K, and large anisotropy in the susceptibility with an easy c axis, but also features of a heavy-fermion system, namely, a large value of χ as $T \rightarrow 0$. The temperature dependence of the resistivity of URu_2Si_2 is qualitatively similar to other heavy-fermion systems, increasing below room temperature to a large maximum at the coherence temperature 70 K, followed by a decrease of more than an order of magnitude.[2,3,10] The resistivity is strongly anisotropic and largest in the plane normal to the easy magnetic c axis.

The main interest in URu_2Si_2 has been that, despite antiferromagnetic fluctuations and order, it undergoes a phase transition to a strongly anisotropic superconducting state below $T_c = 1.2$ K.[1-3] It seems that the magnetic and superconducting properties are closely related in this compound.[11,12]

The present work is primarily concerned with studying the magnetic properties by characterizing the antiferromagnetic ground state and the excitations from it using neutron-scattering techniques. We find that the blend of crystal-field and heavy-fermion properties observed by bulk measurements shows itself as two regimes of magnetic fluctuation behavior. There is a regime of sharp crystal-field-like excitations at low energies for fluctuations propagating in the tetragonal basal plane, whereas at higher energies and for fluctuations propagating perpendicular to this plane the excitations resemble the broad correlated itinerant magnetic fluctuations observed in other heavy-fermion antiferromagnets.

A few experimental studies of magnetic fluctuations in URu_2Si_2 have been reported. Walter *et al.*[13] performed inelastic neutron scattering from a powder sample and showed that the phase transition at $T_N = 17.5$ K is accompanied by the development of a gap in the magnetic excitation spectrum and that the density of low-energy magnetic excitations is peaked at 2.4 THz. Broholm *et al.*[14], by single-crystal neutron scattering, determined the antiferromagnetic order which develops below $T_N = 17.5$ K and showed that the low-energy magnetic excitations are in the form of propagating crystal-field-like excitations. Note that we use the term "crystal-field-like" to describe the existence of a sharp excited state in the magnetic spectrum. Its origin may be crystal-field splitting of a degenerate multiplet of the total angular momentum $J = L + S$ or, in metallic systems, the states resulting from Kondo screening of the J multiplets.

We give a complete account of our single-crystal elastic and inelastic neutron-scattering data, parts of which we have already published.[14,15] Our investigations focus on the phase transition at 17.5 K and on the nature of the low-temperature magnetic fluctuations in URu_2Si_2. The paper is organized in four main parts: sample and experimental technique, experimental results, analysis, and discussion and conclusion.

II. SAMPLE AND EXPERIMENTAL TECHNIQUE

The measurements were performed on a 5-cm-long cylindrical single crystal with a diameter of 0.5 cm, grown by a specially adapted Czochralski method.[16] The as-grown crystal was annealed for 7 days at 1000 °C. URu_2Si_2 has the body-centered tetragonal $ThCr_2Si_2$ structure with lattice parameters $a = 4.124$ Å and $c = 9.582$ Å at 4.2 K. Figure 1 shows a sketch of this structure along with the antiferromagnetic order realized below $T_N = 17.5$ K. Our crystal had an a axis along the cylinder axis, and the measurements were performed with momentum transfers in the $(h0l)$ and $(hk0)$ planes. The crystal was found to have a substantial amount of stacking faults along the tetragonal c axis, giving rise to weak, temperature-independent, nuclear rodlike scattering along this axis. Similar effects were found in another cylindrical single crystal grown along the c axis. The sample was mounted in a copper can packed with copper shavings to ensure good thermal contact. The temperature was monitored using a carbon resistor located inside the sample can.

The neutron-scattering experiments were performed at the cold neutron source at the DR3 reactor of Risø National Laboratory and at the thermal neutron source at the NRU reactor of Chalk River Nuclear Laboratories. We have employed standard triple-axis neutron-scattering techniques with choices of experimental configurations to suit our purposes.

Measurements made at Risø were of excitations below 2.4 THz in the $(h0l)$ plane. The (0,0,2) reflection from pyrolytic graphite (PG) was used as monochromator and analyzer. Be and/or PG filters were used to suppress higher-order contamination of the scattered beam. Measurements at Chalk River were made in the $(hk0)$ plane and at higher energies in the $(h0l)$ plane. Fixed scattered neutron energies in the range 2–5 THz were used with a PG (002) analyzer and a Si(111) monochromator. Many of the scans were performed with a scattered neutron energy of 3.5 THz to permit the use of the PG filter in the scattered neutron beam. Measurements in a magnetic field were performed in the horizontal field magnet cryostat, a Chalk River–Oxford Instruments design, permitting orientation of the field along any crystallographic

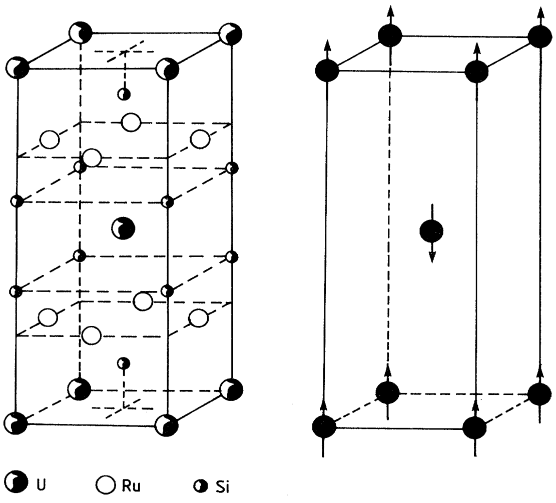

FIG. 1. Diagram on the left shows the crystal structure of URu_2Si_2. The one on the right shows the antiferromagnetic structure of the uranium atoms below $T_N = 17.5$ K.

direction at low temperature.[17] In Table I we summarize the experimental configurations employed. We will refer to this table below by the configuration number in the first column.

III. EXPERIMENTAL RESULTS

In this section we describe the experimental results obtained along with those parts of the data analysis which may be done with a minimum of assumptions. We describe the magnetic ground-state properties and the low-temperature excitations from it, the development of short-range antiferromagnetic correlations in the high-energy overdamped response, and finally the antiferromagnetic phase transition at $T_N = 17.5$ K.

A. Antiferromagnetic order

Figure 2 shows elastic scans along the a^* and c^* directions through the forbidden nuclear (1,0,0) and (1,0,2) Bragg peaks. The data were taken with spectrometer configuration No. 1 of Table I. The main criterion for the choice was a good energy resolution and a minimal $\lambda/2$ contamination of the beam. The dashed line in Figs. 2(a) and 2(b) indicates the nuclear incoherent background measured at 60 K, well above the phase transition at 17.5 K. As discussed more thoroughly in Sec. III E, the scattering develops rapidly at T_N. We have found similar scattering at reflections $(h0l)$, where $h+l=2n+1$, $h\neq 0$. The scattering decreases at high-momentum transfers. These observations are consistent with an approximately static and long-range (although not infinite; see below) antiferromagnetic correlation of the c-axis components of the magnetic-moment density located at the uranium sites. The correlations are such that the moment density associated with each U site is opposed to its four U neighbors displaced above and below it along the c axis as shown in Fig. 1.

Figure 3 shows the integrated magnetic intensity of a selection of these antiferromagnetic peaks in the $(h0l)$ plane, divided by their associated polarization factor. The magnetic part of the scattering was found by subtracting the scattering at 30 K from the low-temperature scattering. The polarization factor associated with spins polarized along the c axis is the squared basal-plane component of the unit vector parallel to the scattering vector. The data are a measure of the squared Fourier transform of the magnetic-moment density associated with the antiferromagnetic peaks. This is found to decrease as a function of momentum transfer with a characteristic half-width comparable to that found in the insulator UO_2 (solid line).[18]

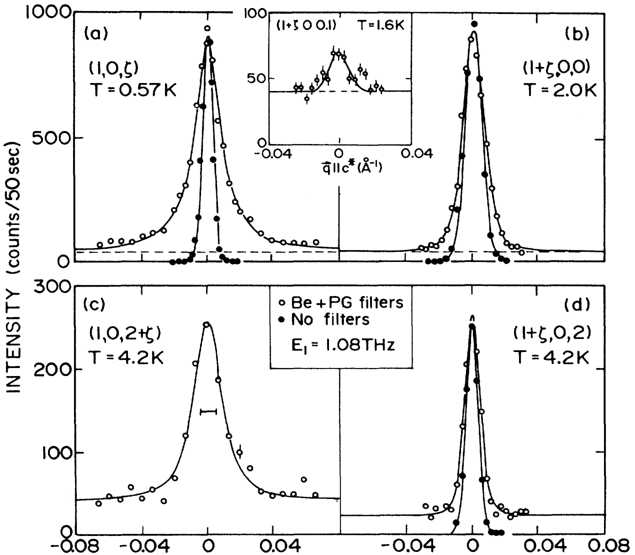

FIG. 2. Elastic scans along the a^* and c^* axes through the antiferromagnetic peaks at (1,0,0) and (1,0,2). The solid circles are taken without filters as a measure of the instrumental resolution. The top inset is a scan across the tails of the peak in (a).

To describe the nature of the antiferromagnetic correlations in more detail, we return to Fig. 2. The scans are taken at various temperatures below 5 K. As we shall

TABLE I. Spectrometer configurations used in our experiments on URu_2Si_2. Fourth column is the fixed final energy. Fifth column is the horizontal collimation in minutes of arc between source and monochromator, monochromator and sample, sample and analyzer, and analyzer and detector, respectively. Sixth and seventh columns indicate crystalline material and Bragg reflection used as monochromater and analyzer. Eigth column gives material used as filter before the analyzer. Be indicates polycrystalline beryllium cooled to 77 K; PG means a pyrolytic graphite crystal with the c axis along the neutron beam. Last column lists full width at half maximum of the incoherent energy resolution.

Configuration No.	Reactor	Instrument	E_f/THz	Collimation	Monochromater	Analyzer	Filter	ΔE/THz
1	Risø-DR3	TAS6	1.1	60'-49'-52'-66'	PG (002)	PG (002)	Be+PG	3.6×10^{-2}
2	AECL-NRU	N5	3.5	54'-66'-60'-120'	Si(111)	PG (002)	PG	0.30
3	AECL-NRU	N5	4.0	54'-40'-64'-120'	Si(111)	PG (002)		0.34
4	AECL-NRU	N5	3.0	40'-60'-60'-120'	Si(111)	PG (002)		0.24
5	AECL-NRU	N5	5.0	40'-60'-60'-120'	Si(111)	PG (002)		0.46
6	Risø-DR3	TAS7	1.1	20'-open-53'-60'	PG (002)	PG (002)	Be+PG	4.6×10^{-2}
7	Risø-DR3	TAS7	1.2	20'-open-open-open	PG (002)	PG (002) focused	Be	6.3×10^{-2}
8	Risø-DR3	TAS7	1.2	20'-open-53'-66'	PG (002)	PG (002)	Be	4.6×10^{-2}

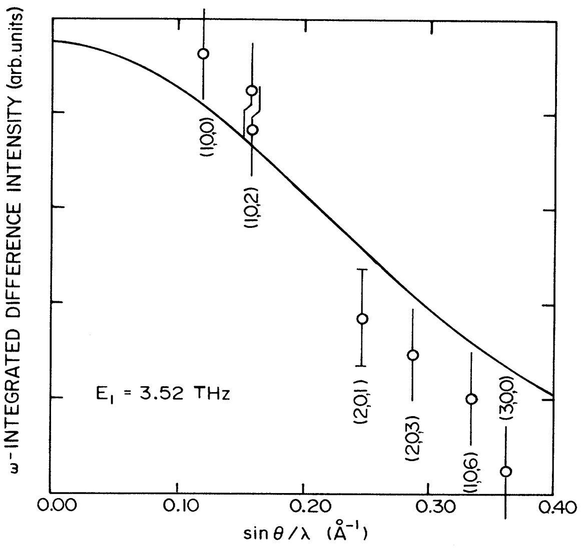

FIG. 3. Integrated difference of elastic scattering between $T=5$ and 30 K at forbidden nuclear reflection $(h0l)$, $h+l=2n+1$, $h=0$. The difference intensity has been divided by a polarization factor as discussed in the text. Half the scattering angle is denoted by θ, and λ is the neutron wavelength. The solid line is a smooth interpolation of neutron-scattering data (Ref. 18) measuring the form factor of UO_2.

later show, the evolution of this antiferromagnetic scattering has essentially ceased at these temperatures, which are well below T_N. We may thus regard the data of Fig. 2 as a measure of the magnetic ground-state properties of our URu_2Si_2 crystal. Since no part of the spectrometer has wavelength-dependent collimation, the instrumental resolution for elastic scattering at (1,0,0) and (1,0,2) can be measured by performing identical scans with an unfiltered neutron beam containing a significant amount of $\lambda/2$ contamination. The scattering in these scans, also shown in Fig. 2, is resolution-limited Bragg scattering of $\lambda/2$ neutrons from the (2,0,0) and (2,0,4) nuclear reflections, respectively. Comparing the line shapes observed for the filtered beam with these data, we conclude that the antiferromagnetic peak in our sample is almost resolution limited in the basal plane, whereas the scans along the c^* axis clearly have a non-Gaussian line shape that is broader than the resolution function.

Caution is necessary when interpreting these experimental facts. The approximate symmetry of the spectrometer about a vertical plane containing the scattering vector in an elastic-scattering process implies that the principal axes of the resolution function in the horizontal plane of momentum space are parallel and perpendicular to the scattering vector. Furthermore, the momentum transfer perpendicular to the scattering vector is most strongly correlated with the energy transfer. This means that a low-energy isotropic response, due to finite-energy resolution, will appear broadened along the perpendicular direction to the scattering vector. In Fig. 2, however, similar line-shape anisotropies are observed around two different antiferromagnetic peaks, namely, (1,0,0) and (1,0,2). It is thus clear that the anisotropy is related to the crystalline directions and not to the transverse and longitudinal direction relative to the scattering vector.

The inset at the top of Fig. 2 further elucidates the rodlike nature of the scattering. It is a scan in the perpendicular direction $(1+\zeta,0,0.1)$ across the tail of the peak in Fig. 2(a). The solid line through the points has the resolution width. It is clear that the tails of the peak along c^* have a rodlike character, remaining almost resolution limited along the in-plane direction.

To quantify correlation lengths and the size of the ordered moment, a model for exponential decay of correlation in only one dimension, namely, along the c^* axis, is relevant since the peaks are broadened mostly along that direction:

$$\langle S_R^c S_{R+r_c}^c \rangle \sim \exp(-\kappa_c r_c) \ . \tag{1}$$

The corresponding Fourier-transformed correlation function is[19]

$$\langle S_q^c S_{-q}^c \rangle = \langle S^c \rangle^2 \frac{\sinh(\kappa_c c)}{\cosh(\kappa_c c) - \cos(q_c c)} \ . \tag{2}$$

To compare with the measured neutron intensities, the cross section was convoluted with the spectrometer resolution. The independently measured flat nuclear incoherent background and a resolution-limited Gaussian describing the weak contamination of $\lambda/2$ nuclear Bragg scattering were also added. The lines through the data of Fig. 2 are the results of least-squares fits of this model to the data. The inverse correlation lengths deduced from scans around (1,0,0) and (1,0,2) are indistinguishable within experimental accuracy: $\kappa_c(1,0,0)=(9.8\pm0.4)\times10^{-3}$ Å^{-1} and $\kappa_c(1,0,2)=(8\pm1)\times10^{-3}$ Å^{-1}.

Applying the same formalism to the scan along the a^* direction, we deduce inverse correlation lengths of $\kappa_a(1,0,0)=(3.2\pm0.2)\times10^{-3}$ Å^{-1} and $\kappa_a(1,0,2)=(1.7\pm0.3)\times10^{-3}$ Å^{-1}. Thus the anisotropy in the correlations is about a factor of 4. Since the antiferromagnetic scattering along a^* is just barely broader than the resolution widths, the determination of the in-planar correlation is somewhat uncertain. As discussed in the last paragraph of Sec. IV A, there is a reason to believe that these results for the correlation lengths are not intrinsic to URu_2Si_2, but rather arise from defects such as stacking faults in our sample.

The size of the moment was obtained by normalization of the magnetically scattered neutron intensity to the intensity associated with the known cross section of the nuclear (1,0,1) Bragg peak. Since the scattering angle for the (1,0,0) and (1,0,1) reciprocal lattice points are similar, we can neglect the variation of the spectrometer resolution function in this comparison. We found from Fig. 2(a) that $\langle S^c \rangle=(0.04\pm0.01)\mu_B$. To access the energy scale associated with this antiferromagnetic scattering, we performed energy scans at various momentum transfers displaced along the c axis from (1,0,2) at $T=4.2$ K. All these scans had an energy width below 0.02 THz, which is close to that of a Bragg peak. Any finite-energy scale related to this antiferromagnetic scattering is thus more than an order of magnitude less than that of the zone-center spin-wave gap (see below).

B. Low-energy propagating excitations

The excitations from this weak antiferromagnetic ground state were studied by inelastic magnetic neutron scattering using standard triple-axis techniques. Figure 4 shows energy scans at $T=1$ K$\ll T_N$ at various fixed-momentum transfers along $(1,\zeta,0)$. In contrast to other antiferromagnetic heavy-fermion systems,[20] well-defined peaks as a function of energy occur in all these scans. The data of Fig. 4 are in fact resolution limited. This was in general found to be the case when the deviation of momentum transfer from an antiferromagnetic zone center $\mathbf{q}$ was in the basal plane. In contrast, as shown in Fig. 5, for $\mathbf{q}=(0,0,\zeta)\|\mathbf{c}^*$, there is a broadening and a precipitous decrease in intensity of the peak when $|\mathbf{q}|$ increases. In both sets of data the excitation energy depends on $\mathbf{q}$ and the energy and momentum transfer at which peaks occur define the dispersion relation for the magnetic excitations. In Fig. 6 we show the dispersion relation along three high-symmetry directions determined from constant-Q scans such as those of Figs. 4 and 5.

By studying the integrated intensity of equivalent magnetic excitations in different Brillouin zones, we found that the magnetic excitations are polarized along the tetragonal c axis and have a form factor typical for $5f$ electrons. We shall refer to the inelastic scattering as longitudinal since it is polarized along the ordered moment. Normalizing the spin-wave scattering at (1,0,0) to the longitudinal-acoustic-phonon scattering close to (2,0,0) yields a large transition-matrix element of $g\mu_B|\langle 0|J^z|1\rangle|=1.2\mu_B$.[15] The wave-vector dependence of the integrated spin-wave intensity divided by the polarization and form factor of the response is shown in Fig. 7.

The longitudinal nature of the response and the largeness of the inelastic transition-matrix element as com-

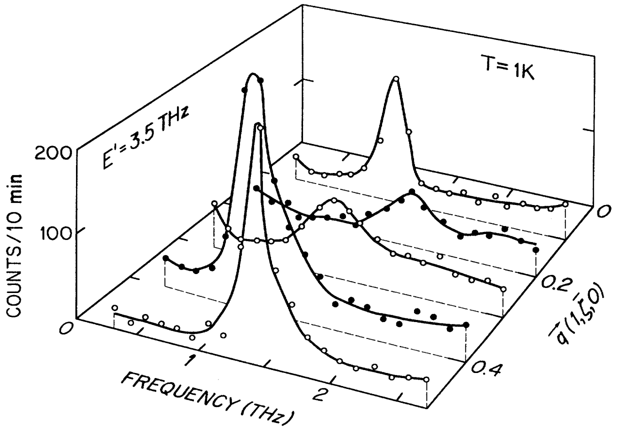

FIG. 4. Constant-Q scans along the $(1,-\zeta,0)$ direction showing resolution-limited magnetic excitations in the basal plane. The data were obtained with configuration No. 2 of Table I. Solid and open symbols are used for clarity of presentation. The lines are guides to the eye.

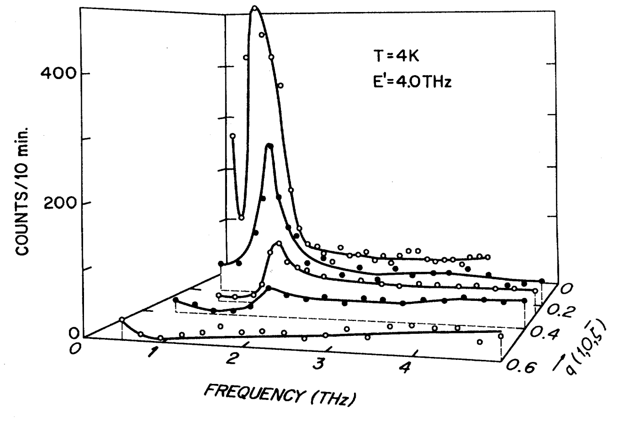

FIG. 5. Constant-Q scans along the $(1,0,-\zeta)$ direction. The intensity of the spin waves decreases precipitously with increasing ζ, and their width increases. The data were obtained with configuration No. 3 of Table I. Solid and open symbols are used for clarity of presentation. The lines are guide to the eye.

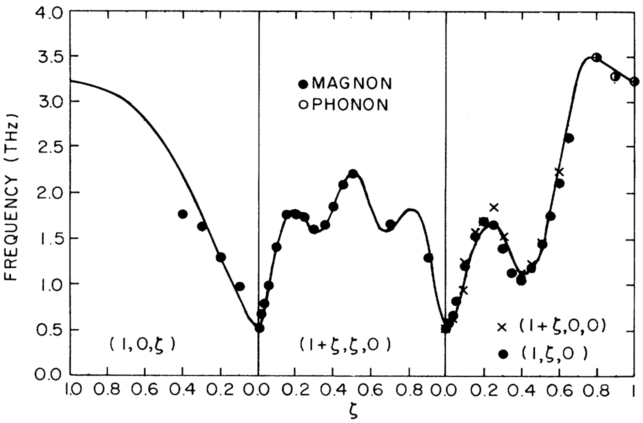

FIG. 6. Measured dispersion of excitations in $\mathrm{URu_2Si_2}$ along the $(1,0,\zeta)$, $(1+\zeta,\zeta,0)$, and $(1,\zeta,0)$ directions. The lines are the results of the fit described in the text.

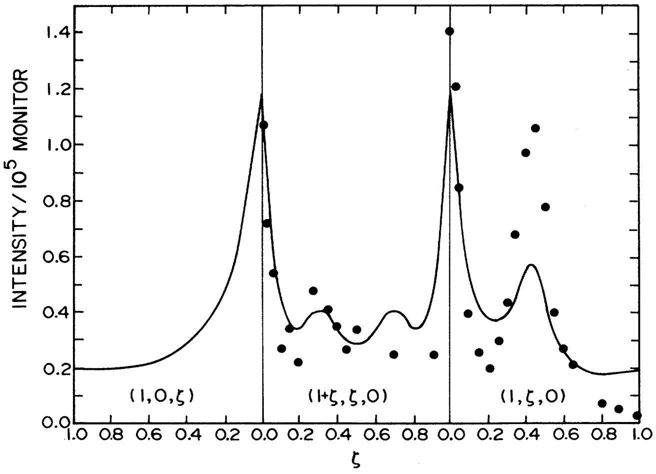

FIG. 7. Wave-vector dependence of the integrated spin-wave intensity divided by the polarization factor $(1-q_c^2)$ for $\mathrm{URu_2Si_2}$.

pared with the elastic scattering from the ordered magnetic structure suggest that the excitations are between two singlet states. To corroborate this conclusion we performed constant-Q scans at (1.5,0,0) in zero magnetic field and in a field of 3 T applied along the c axis. This is the "soft" magnetic axis along which the ordered moment and low-energy magnetic excitations are polarized. If the excited state was degenerate with an associated dipolar matrix element $g\mu_B|\langle 1|J^z|1'\rangle| \approx 2\mu_B$, the excitation would be split by an amount $g\mu_B|\langle 1|J^z|1'\rangle H \approx 2\mu_B H \approx 0.1$ THz in an applied field of 3 T. The result of the measurement is shown in Fig. 8. No broadening beyond the resolution width of 0.4 THz occurs upon application of $H=3$ T. This result confirms that the inelastic peak arises from transitions between two singlets. The temperature dependence of the antiferromagnetic Bragg peak intensity under the same two conditions of applied field is shown in Fig. 9. The size of the ordered moment is reduced by as much as 25% in a 3-T field, although the temperature dependence is unchanged. This reduction in the size of the ordered moment is also characteristic of singlet ground-state systems with induced moment ordering. The applied field suppresses the moment on the antiparallel sublattice, which reduces the molecular field on the parallel sublattice more than the external field enhances it. This leads to an overall reduction of the ordered moment.

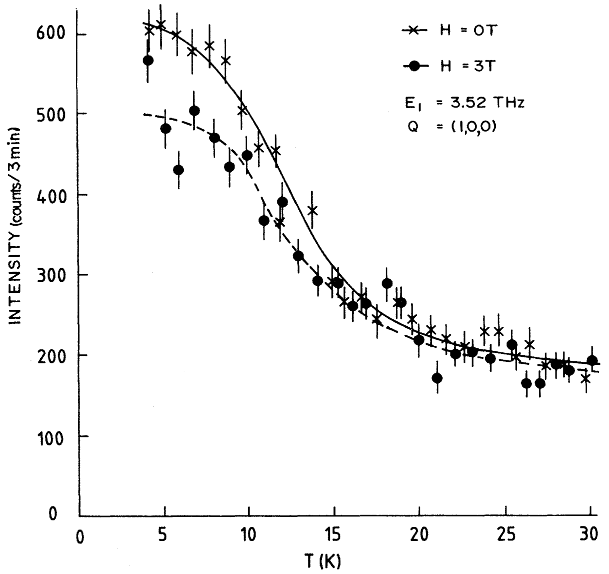

FIG. 9. Temperature dependence of the (1,0,0) antiferromagnetic Bragg peak intensity in zero field and with $H=3$ T applied along c.

C. Overdamped response

We now consider the low-temperature magnetic excitations at energies well above the propagating excitations described above. Figure 10 shows four constant-Q scans taken with the experimental configuration No. 4 of Table I. With this configuration we could resolve the cross section associated with the low-energy dispersive excitations discussed above and still obtain an appreciable count rate from the high-energy continuum response which we shall now discuss.

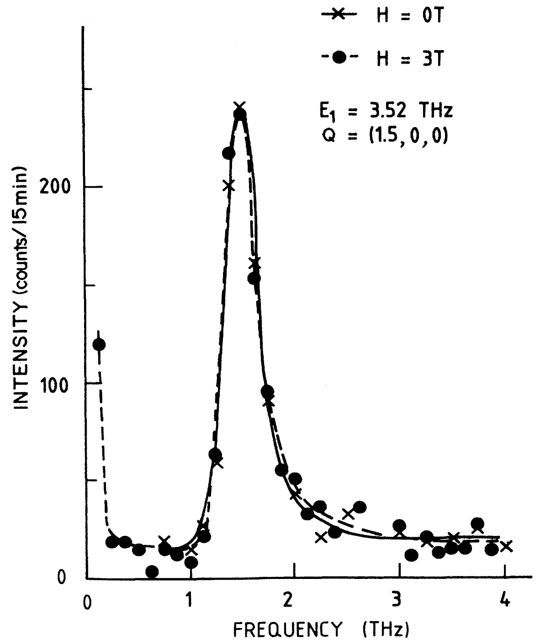

FIG. 8. Constant-Q scan at (1.5,0,0) in zero field and with $H=3$ T applied along c. The lack of any broadening or splitting confirms that the spin waves arise from transitions between two singlets.

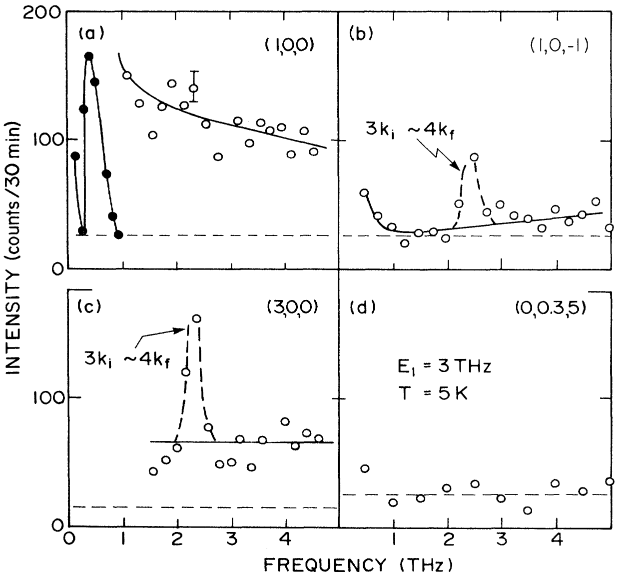

FIG. 10. Low-temperature energy scans at four different reciprocal lattice points taken with configuration No. 4 of Table I. Solid points in (a) are reduced by a factor of 10. The lines through the data are guides to the eye. The dashed line is the background as measured with the analyzer turned away from reflection. The peaks in (b) and (c) arise from a spurious process involving third-order neutrons.

Figure 10(a) shows a constant-Q scan at the antiferromagnetic zone center $\mathbf{Q}=(1,0,0)$. Apart from the low-energy zone-center excitation, discussed in Sec. III B, the count rate from 1 to 5 THz is clearly well above the background. To investigate the origin of this scattering, we performed a similar scan [Fig. 10(c)] at (3,0,0). The translational symmetry of the uranium lattice ensures that the magnetic scattering has the same spectrum here as at (1,0,0). Apart from a spurious process involving higher-order neutrons, the level of scattering at (3,0,0) has decreased significantly as compared with that at (1,0,0). This observation is consistent with the scattering at (1,0,0) being primarily magnetic in origin. The decrease in the scattering at larger momentum transfer reflects the decrease in the magnetic form factor. Phonon scattering, on the other hand, is proportional to the square of the momentum transfer and therefore increases with increasing Q.

An energy scan at (0,0,3.5) is shown in Fig. 10(d). Because of the dipolar nature of the magnetic neutron scattering, the only contribution to the magnetic scattering at this momentum transfer arises from the spin components in the basal plane of the tetragonal structure. We conclude that there is no magnetic scattering from basal-plane spin components in the investigated energy region. With respect to the tetragonal uranium lattice, $\mathbf{Q}=(0,0,3.5)$ is symmetrically equivalent to $\mathbf{Q}=(1,0,0.5)$. As shown below, the scattering at (1,0,0.5) is reduced by a factor of 2 from that at (1,0,0). Had the scattering been isotropic, one would expect the $\mathbf{Q}=(0,0,3.5)$ scan to be similar to the (1,0,0) scan, albeit reduced by a factor of 2. The complete absence of scattering at $\mathbf{Q}=(0,0,3.5)$ therefore shows that there is a strong anisotropy in the high-energy excitation response; i.e., the scattering arises from magnetic fluctuations oriented along the c axis and the ordered moment.

Figure 10(b) shows an energy scan at $\mathbf{Q}=(1,0,1)$. Since this is an allowed nuclear Bragg peak of the body-centered tetragonal structure, the magnetic scattering here arises from in-phase fluctuations of the magnetic-moment density associated with each uranium atom. Apart from the higher-order spurious process at an energy transfer of around 2.4 THz, there is very little magnetic scattering in the form 1.2 to 4.8 THz. The spectrum of Fig. 10(a) is thus specific for flucturations of the same symmetry as the static antiferromagnetic order described in Sec. III A.

Figure 11 shows a constant-energy scan at an energy transfer of 4.1 THz. Momentum transfer is varied along the $(1,0,\zeta)$ direction through the antiferromagnetic zone center (1,0,0). The scan connects the energy scans at the top of Fig. 10. The high-energy response decreases when varying momentum transfer from probing antiferromagnetic fluctuations at (1,0,0) to ferromagnetic fluctuations at (1,0,1) and $(1,0,-1)$. From the width of the peak in this scan, we conclude that the correlation length associated with the magnetic fluctuations probed in Fig. 10(a) is only about one lattice unit.

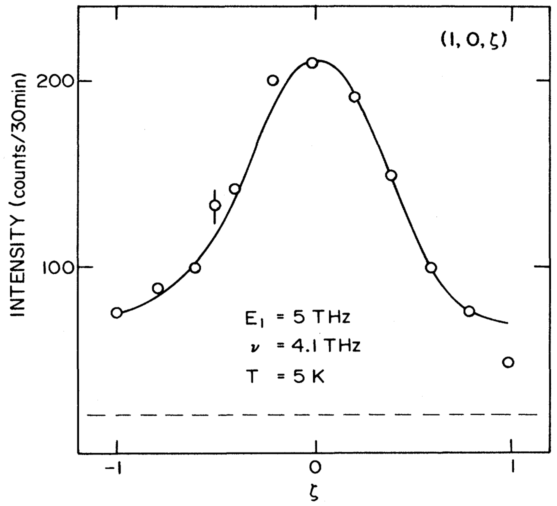

FIG. 11. Constant-frequency scan at 4.1 THz in the ordered phase of URu_2Si_2 through the antiferromagnetic zone center at (1,0,0). The data were obtained with configuration No. 5 of Table I. The dashed line is the background measured with analyzer turned. The solid line is a guide to the eye.

To illustrate the crossover from the low-energy propagating response to the high-energy overdamped response, Fig. 12 shows data from both regions of energy and momentum transfer taken with configuration No. 4 of Table I. The data are displayed in a three-dimensional (3D) perspective as a function of energy transfer and momentum transfer along the $(1,0,\zeta)$ direction. The data should be studied with reference to the dispersion relations of the propagating excitations shown in Fig. 6. The peak at 0.5 THz corrresponds to the divergent response at the minimum zone-center energy. At slightly higher energies around 1 THz, a double-peak structure emerges, corresponding to the two equivalent directions of propagation, $(1,0,\zeta)$ and $(1,0,-\zeta)$. The asymmetry in the data at this energy is due to a resolution effect. Final-

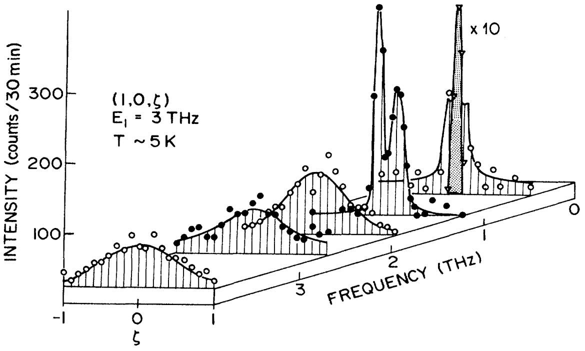

FIG. 12. Prespective view of the scattered neutron intensity vs energy transfer and momentum transfer along $(1,0,\zeta)$. The data are taken in the ordered phase at $T=5$ K. The asymmetry in the double-peak structure is due to a resolution effect. The solid lines are guides to the eye. Solid and open symbols are used for clarity of presentation. At $\nu=0.5$ THz the data plotted as triangles which define the hatched region has been reduced by a factor 10.

ly, above 1.2 THz the continuous spectrum of antiferromagnetically correlated spin fluctuations emerges. The data of Fig. 12, in which both a divergent and a continuous part of the spectrum are resolved, prove that the broad part of the response does not arise from unresolved sharp features such as high-velocity spin waves. Finally, we note that similar high-energy features have been observed at other high-symmetry points in the $(h0l)$ plane, but are currently not as well documented as the scattering described above.

D. Development of antiferromagnetic correlation below $T \sim 100$ K

We now turn to the temperature dependence of the high-energy antiferromagnetic fluctuations. Figure 13 shows the energy scan at (1,0,0) for three different tematures. As discussed in detail in Sec. III E, the low-energy propagating response becomes heavily damped above the phase transition at $T_N = 17.5$ K. From Fig. 13(b) it is, however, evident that the intensity of inelastic scattering beyond 1.5 THz remains almost unaffected by this transition to temperatures as high as 40 K. This rules out the interpretation of the continuous high-energy response as arising from two-magnon scattering or having significant contributions from the incomplete resolution of the intense low-energy peak at 5 K. Had this been the case, the high-energy scattering would undergo substantial changes at the 17.5-K phase transition. Upon raising the temperature from 40 to 80 K, the inelastic scattering decreases slightly and most predominantly at low energies. Recall that from the fluctuation dissipation theorem, the inelastic magnetic neutron scattering is proportional to

$$S(\mathbf{Q},\nu) = [1 + n(\nu)]\chi''(\mathbf{Q},\nu) , \tag{3}$$

where $\chi''(\mathbf{Q},\nu)$ is the imaginary part of the generalized susceptibility characterizing the response of the magnet to spatially and temporally varying external fields. The detailed balance factor $1 + n(\nu) = [1 - \exp(-\beta h\nu)]^{-1}$ increases roughly proportional to $T = 1/k_B\beta$ for $\nu < 1.5$ THz upon heating from 40 to 80 K. The near temperature independence of the inelastic scattering in this energy range therefore implies that $\chi''(\mathbf{Q},\nu)$ is decreasing substantially upon heating, thus compensating this effect.

To quantify this development we fit the data at 40 and 80 K to the single imaginary pole susceptibility $\chi(\mathbf{Q},\nu) = \chi_Q\Gamma_Q/(\Gamma_Q - i\nu)$. This form has been the successful basis of similar analysis in a variety of heavy-fermion and itinerant magnets. The solid lines in Fig. 13 are best fits of (3) to the data with the independently measured background added. At both temperatures the simple form for $\chi''(\mathbf{Q},\nu)$ adequately accounts for the data, and we find that the characteristic energy scales for magnetic fluctuations at $\mathbf{Q} = (1,0,0)$ increases from 1.9 ± 0.1 THz at 40 K to 3.5 ± 0.3 THz at 80 K. Our fits also determine the ratio

$$\chi_{(1,0,0)}\Gamma_{(1,0,0)}(T = 40\text{ K})/\chi_{(1,0,0)}\Gamma_{(1,0,0)}(T = 80\text{ K}) = 0.9 \pm 0.1 ,$$

implying that the product $\chi_{(1,0,0)}\Gamma_{(1,0,0)}$ is only weakly temperature dependent between 40 and 80 K. Although the single imaginary pole susceptibility can account for the magnetic fluctuations above T_N, the inelastic magnetic scattering below T_N is not simply a superposition of such scattering with that associated with dispersive crystal-field levels. Figure 12 clearly shows that at $\nu = 1$ THz the inelastic magnetic scattering is exhausted by crystal-field-like excitations with no indications that the weakly Q-dependent scattering which dominates at $\nu = 2$ THz persists.

The increase of the fluctuation rate at the antiferromagnetic zone center upon heating is an indication that the antiferromagnetic correlations of the magnetic fluctuations depicted in Figs. 11 and 12 decrease at higher temperatures. To establish this we have measured two characteristic points in (q,ν) space as a function of temperature. The results are illustrated in Fig. 14. This figure shows the scattered neutron intensity at an energy transfer of 1.9 THz at $\mathbf{Q} = (1,0,1)$ and (1,0,0). The two reciprocal lattice points correspond to the extremal points in the scan displayed in Fig. 11. From Fig. 14 it is clear that, whereas the inelastic scattering at $\mathbf{Q} = (1,0,0)$ decreases slightly with increasing temperature, the

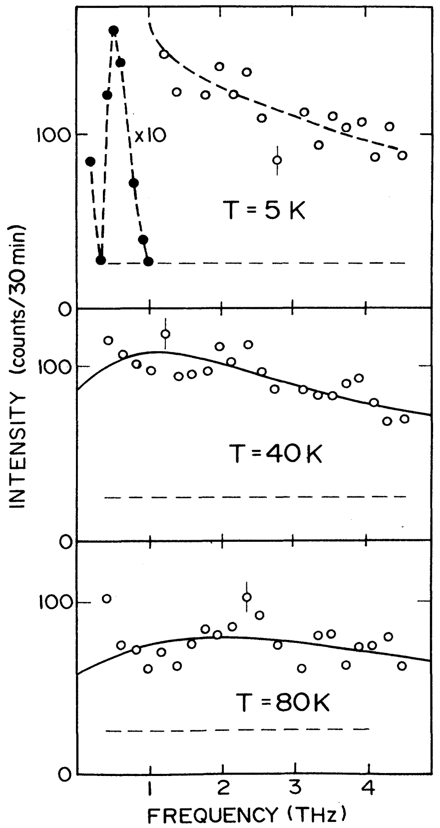

FIG. 13. Energy scans at the antiferromagnetic zone center at three different temperatures obtained with configuration No. 4 of Table I. Solid symbols have been reduced by a factor of 10. The dashed line is the background as measured with the analyzer turned away from reflection. The full lines are guides to the eye.

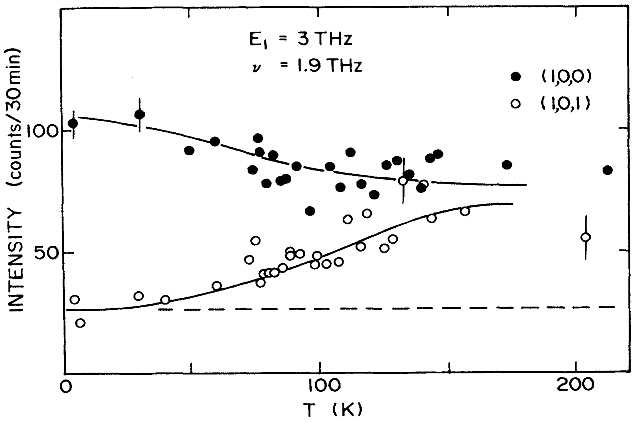

FIG. 14. Scattered neutron intensity vs temperature at an energy transfer of 1.9 THz and scattering vectors (1,0,0) and (1,0,1). The dashed line is the analyzer-turned background. The solid lines are guides to the eye. The data were taken with configuration No. 4 of Table I.

scattering at Q=(1,0,1) increases rapidly such that above 100 K the intensity at the two reciprocal lattice points becomes similar. Antiferromagnetic correlations of the high-energy overdamped response thus only are apparent below 100 K. It is interesting to note that the development of antiferromagnetic correlations roughly coincides with the temperature below which the resistivity of URu_2Si_2 begins to decrease.

E. Antiferromagnetic phase transition

The weak elastic antiferromagnetic peaks described in Sec. III A appear at temperatures below the phase transition at $T_N = 17.5$ K.[1] Figure 15 shows the temperature dependence of the integrated intensity of θ-2θ scans through the antiferromagnetic peak at (1,0,0). The data were obtained using configuration No. 6 of Table I, this provides minimal $\lambda/2$ contamination and an energy resolution of 4.6×10^{-2} THz, which discriminates against the large inelastic cross section when the spectrometer is set for elastic scattering. As described later in this section, this inelastic magnetic scattering is heavily damped and extends all the way to $\nu=0$ above T_N. Within the resolution volume of this experiment, the inelastic scattering extrapolated to $\nu=0$ throughout the temperature region covered only contributes a count rate less than 5% of the low-temperature antiferromagnetic peak intensity. The temperature-dependent scattering studied here is a distinct, approximately elastic, component of the antiferromagnetic zone-center scattering even in the immediate vicinity T_N.

Figure 16 shows data taken at Q=(1,0.4,0) where the intensity of the magnetic excitation is largest above T_N. The excitation spectrum develops from a broad hump of antiferromagnetically correlated, heavily damped, response in the paramagnetic phase to an almost resolution-limited peak which is largely unaffected by the superconducting phase transition at $T_c = 1.2$ K.

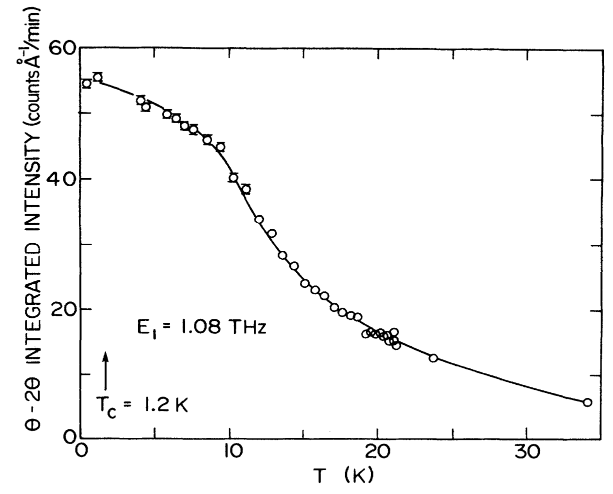

FIG. 15. Integrated elastic magnetic scattering at (1,0,0) as a function of temperature. The c^* axis was perpendicular to the scattering plane in this experiment.

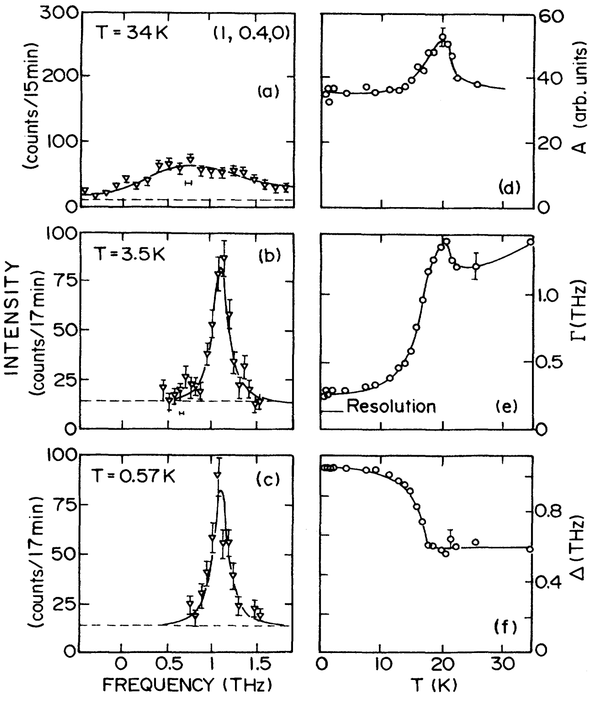

FIG. 16. Constant-Q scans at (1,0.4,0) in (a) the paramagnetic, (b) the antiferromagnetic, and (c) the superconducting phase. The data in (a) were obtained with configuration No. 7, that of (b) and (c) with configuration No. 8. Data taken with different configurations have been normalized and plotted so that equivalent cross sections correspond to the same height over the background. The solid lines in (a)–(c) are fits as described in the text, and (d)–(f) show the temperature dependence of the three parameters obtained from fits to data similar to (1). The lines through these points are guides to the eye.

We have summarized a series of scans similar to Fig. 16(a) as a function of temperature on the right-hand side of the figure. Here we show the temperature dependence of the amplitude A, damping Γ [full width at half maximum (FWHM)], and first moment Δ, of a resolution- and background-corrected Lorentzian response which describes the data well. The abrupt temperature dependence of Γ and Δ at T_N coincides with the anomaly at this temperature in the heat capacity.

IV. ANALYSIS AND DISCUSSION

It is clear from Sec. III B that the low-energy magnetic excitation spectra in URu_2Si_2 at low temperatures bear striking similarities to those of conventional rare-earth systems. Here it is usual to treat the $4f$ electrons as essentially perfectly localized and subject to interatomic correlations, which constrict their motion within the Hund's rule ground-state multiplet.[21] Also, many of the bulk properties of URu_2Si_2 seem to be governed by the same underlying physics as is known from rare-earth magnetism.[22] We mention briefly the strongly anisotropic susceptibility and its Schottky-like anomaly at 50 K,[1] and the high-field magnetization data,[5] which show steplike magnetization increases in the field around 35 T.

There are, however, as described in Sec. III C, features in the high-energy magnetic response which cannot be explained by conventional spin-wave and crystal-field theories. Features in the bulk properties, such as the heavy-fermion linear specific-heat term [$\gamma = 50$ mJ/(mol K^2)] (Ref. 1) and the increasing resistivity as temperature is decreased from room temperature, also suggest that we cannot accommodate the properties of URu_2Si_2 within this simple model. However, we believe that despite these important discrepancies, we can use the conserved local-moment model as a means of parametrizing dispersion relations and gap energies and conveniently relating these to some key bulk properties.[22,23] To some extent this can even be done without relying on assumptions known to be doubtful.

A. Applying crystal-field theory to URu_2Si_2

One can argue that the resonant low-energy spin response *proves* that there exist in URu_2Si_2 dipolar moments whose size is an approximately conserved quantity in the motion of the unpaired $5f$ electrons. The absence of broadening or splitting of the magnetic excitations upon application of a field shows that the ground and first excited states are both singlets. This means that an even number of electrons must be accommodated in $5f$ states of the U atom. An uneven number would give rise to a Kramers-doublet ground state. Of the two ionization levels in which uranium most frequently occurs, U^{4+} and U^{3+}, we can therefore exclude the latter and conclude that *two* $5f$ electrons remain essentially localized about each uranium atom. The corresponding Hund's rule ground-state $^3H_4$ is ninefold degenerate. From group theory two rigorous results are available. First, electrostatic interactions with tetragonal symmetry split the $^3H_4$ state into five singlets and two doublets. Second, the only allowed longitudinal transitions within these seven energy levels are between singlet states. The latter result is consistent with our experimental data.

Although a singlet ground state has no moment, interactions between sites can cause mixing between the ground and first excited states, resulting in an induced moment transition.[24] The magnitude of the ordered moment then depends on the balance between the intersite interaction and splitting of the levels. To model our low-energy resonant magnetic excitations data, we consider only the two lowest-lying singlet states. A singlet-singlet level scheme as described by Wang and Cooper[25] has already been used with some success to describe the bulk magnetic and thermal properties of URu_2Si_2.[22,26]

In the random-phase approximation the interacting susceptibility of the singlet-singlet model in the ordered state is given by

$$\chi_q^{zz}(\omega) = \frac{2\tilde{\Delta}\tilde{\alpha}^2 f_{01}}{\omega_q^2 - \omega^2} . \tag{4}$$

The wave-vector dependence of the spin-wave energy is

$$\omega_q = [\tilde{\Delta}^2 - 4\tilde{\alpha}^2 \tilde{\Delta} J(\mathbf{q}) f_{01}]^{1/2} , \tag{5}$$

where $\tilde{\Delta}$ is the splitting of the two singlets, $\tilde{\alpha} = g\mu_B |\langle \tilde{0} | S^z | \tilde{1} \rangle|$, and

$$f_{01} = \tanh(\beta\tilde{\Delta}/2) . \tag{6}$$

The tilde indicated renormalization of parameters from their value in the paramagnetic state caused by the magnetic ordering. $J(\mathbf{q})$ is the Fourier transform of the interactions between sites:

$$J(\mathbf{q}) = \sum_j J(\mathbf{r}_j) \exp(i\mathbf{q}\cdot\mathbf{r}_j) . \tag{7}$$

The imaginary part of (4), to which the neutron-scattering cross section is proportional, is

$$\mathrm{Im}[\lim_{\varepsilon \to 0^+} \chi_q^{zz}(\omega + i\varepsilon)] = \pi \frac{\tilde{\Delta}}{\omega_q} \tilde{\alpha}^2 f_{01} [\delta(\omega_q - \omega) - \delta(\omega_q + \omega)] . \tag{8}$$

In order to characterize adequately the observed dispersion and intensities of the excitations, seven exchange constants are required. The lines in Fig. 6 and 7 are the result of the fit. The agreement for the dispersion is quite good, and the intensities are in fair agreement. The value for the splitting of the singlets, $\tilde{\Delta}$, is 2.4 THz (~ 115 K), in good agreement with the value extracted from specific-heat measurements (130 K).[2,27]

The dependence of the extracted exchange constants on distance is shown in Fig. 17. They are ferromagnetic at large distances, but antiferromagnetic at short distances. Such an oscillatory behavior for the spatial dependence of the exchange constant is expected for the Ruderman-Kittel-Kasuya-Yosida (RKKY) interaction in a metallic antiferromagnet. For example, the line in Fig. 17 corresponds to the conventional spherically symmetric RKKY interaction

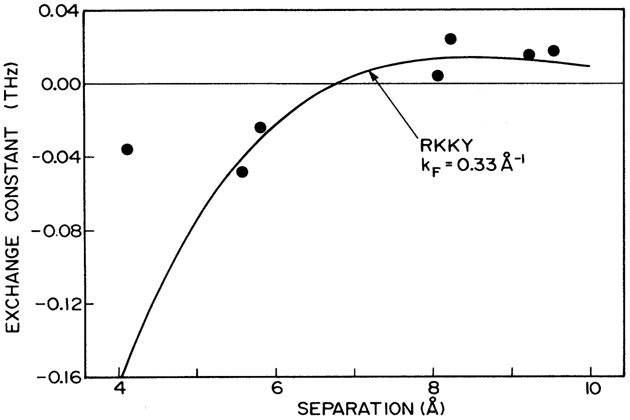

FIG. 17. Distance dependence of the exchange constants derived from the spin-wave data. The line is the standard spherically symmetric RKKY interaction with $k_F=0.3$ Å^{-1}.

$$J(r)=A[\cos x-(\sin x)/x]/x^2 \quad (x=2k_F r)\ , \tag{9}$$

where $k_F=0.3$ Å^{-1}.

It is also possible to calculate the matrix-element-weighted spin-wave density of states for the singlet-singlet model:

$$\rho'(\omega) \propto \sum_q \pi \frac{\tilde{\Delta}}{\omega_q} \tilde{\alpha}^2 f_{01} \delta(\omega-\omega_q)\ . \tag{10}$$

Figure 18 shows the results of this calculation using our data. This calculation does not take into account the broad spectrum of magnetic excitations at higher energies and, therefore, must be regarded as a first approximation. Also shown in Fig. 18 is the observed real part of the infrared optical conductivity.[28] The similarity between the matrix-element-weighted density of spin-wave states and the infrared measurement, which probes charge excitations, suggests that the spin and charge fluctuations are strongly coupled together in this system. The same conclusion is reached when comparing the infrared optical conductivity data to the unweighted spin-wave density of states: $\rho(\omega) \propto \sum_q \delta(\omega-\omega_q)$.

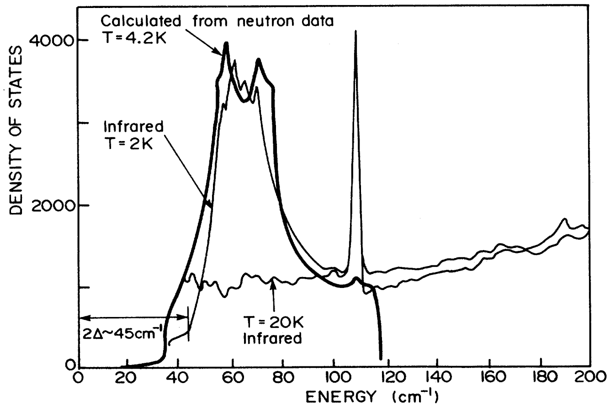

FIG. 18. Calculated spin-wave density of states (thick line). The thin lines are the measured real part of the infrared optical conductivity (Ref. 28) at 2 and 20 K. The similarity between the two suggests that the magnetic excitations are strongly coupled to the charge excitations.

The singlet-singlet model gives a reasonable description of the low-temperature resonant magnetic excitation spectrum, but as we show in the following, it falls short in accounting for other important magnetic properties of URu_2Si_2 such as the small ordered moment and bulk susceptibility. By normalizing the resonant inelastic magnetic scattering at (1,0,0) to longitudinal-acoustic-phonon scattering near (2,0,0), we find that[15]

$$\pi \frac{\tilde{\Delta}}{\omega_{(1,0,0)}} \tilde{\alpha}^2 f_{01} \approx 24\mu_B^2\ . \tag{11}$$

Inserting $\omega_{(1,0,0)}=0.43$ THz, $\tilde{\Delta}=2.4$ THz, and $f_{01}=1$, we obtain $\alpha=1.2\mu_B$. The fact that the ordered moment is almost two orders of magnitude smaller than this cannot be accounted for by the singlet-singlet model. Solving the self-consistent mean-field equations for the ordered moment at $T=0$ yields[29]

$$\langle m_{q0} \rangle = \alpha(1-1/\eta^2)^{1/2}\ , \tag{12}$$

where

$$\eta = \frac{4J(\mathbf{q}_0)\alpha^2}{\Delta}\ . \tag{13}$$

In this expression α and Δ are the transition-matrix element and energy splitting of the singlet levels in the *paramagnetic* state. These are related to the renormalized parameters which we may deduce from the measured dispersion relation by $\tilde{\alpha}=\alpha/\eta$ and $\tilde{\Delta}=\eta\Delta$. Inserting in (13) and solving for $1/\eta^2$, we obtain

$$\frac{1}{\eta^2} = \frac{4J(\mathbf{q}_0)\tilde{\alpha}^2}{\tilde{\Delta}} = 1 - \left[\frac{\omega_{q0}}{\tilde{\Delta}} \right]^2 , \tag{14}$$

where (5) evaluated at $\mathbf{q}=\mathbf{q}_0$ has been used in the last equality. Substituting (14) into (12), we obtain

$$\langle m_{q0} \rangle = \tilde{\alpha} \frac{\omega_{q0}}{\tilde{\Delta}}\ . \tag{15}$$

Inserting previously quoted experimentally determined values yields the mean-field estimate of the ordered moment, $\langle m_{q0} \rangle = 0.2\mu_B$, which is nearly an order of magnitude larger than the measured ordered moment.

There are several possible origins of this discrepancy. First, the statics and dynamics of singlet–ground systems is still an open subject,[30] and in particular only few experimental realizations exist. In Pr_3Tl, which is a *ferromagnetic* singlet-triplet system,[29] the random-phase approximation (RPA) and mean-field theory reproduced the measured dispersion in the ordered state given the experimentally determined magnitude of the ordered moment. On the other hand, in PrSb, a singlet-triplet system which is a type-I antiferromagnet at high pressures, the phase-transition does not proceed through a soft-mode transition as predicted by RPA theory.[31] To our knowledge URu_2Si_2 is the first antiferromagnetic singlet-singlet system to be discovered. It may therefore well be that the lack of consistency between the dynamic and static aspects of our model calculation lie in the inadequacy of the RPA and mean-field approximations rather than the singlet-singlet model itself.

A second possible explanation within crystal-field theory is that the singlet-singlet level scheme is in fact oversimplified. Our neutron-scattering experiments only show evidence for two low-energy crystal-field levels, but that does not rule out the existence of resonant levels which are not coupled to the ground state by the dipolar operator and therefore are unobservable by our experiments. The temperature dependence of the bulk susceptibility of URu_2Si_2, which shows a maximum at $T=50$ K$\sim 3T_N$, in fact *cannot* be reconciled with a singlet-singlet level scheme: In a singlet-singlet system the susceptibility in the paramagnetic regime is a monotonically decreasing function of temperature through its dependence on the population difference of the two levels. At least three dipolar active levels are required to give rise to a susceptibility maximum in the paramagnetic state. A low-energy crystal-field scheme which does have a maximum in the susceptibility above T_N and is consistent with our neutron-scattering data consists of three singlets, A_2, A_1, and A_2, with forbidden dipolar transition between the ground- and excited-state singlets of A_2 symmetry. The highest-lying singlet can thus only be observed by neutron scattering as transitions from the excited state A_1 when a significant population exists in the excited state. The cross section corresponding to this transition would only be appreciable in a temperature interval from about 50 to 150 K. Although Fig. 13 does not show any sharp level in this regime, disfavoring this scenario, we have not made an exhaustive search for a cross section of this nature.

Finally, it is possible that the phase-transition at $T_N=17.5$ K cannot be viewed as a simple rearrangement of crystal-field levels inducing an antiferromagnetic moment in the ground state. In particular, a variety of data including our high-energy magnetic neutron-scattering results suggest that we must regard the singlet levels as effective levels resulting from the hybridization of $5f$ electrons with itinerant electrons. The modification of this hybridization could well be an integral part of the phase transition, in which case crystal-field theory is clearly an inadequate model.

Not only the small magnitude of the antiferromagnetic moment is anomalous, but the antiferromagnetic correlations are two dimensional since the correlation length along the c^* axis remains finite down to the lowest temperature (0.6 K) accessed in this experiment. As previously mentioned, we observed temperature-independent rodlike nuclear scattering along the c^* axis of our crystal, indicating the presence of stacking faults. Most likely, such crystalline imperfections are responsible for limiting the antiferromagnetic correlation length along the c^* axis of our sample. This interpretation is consistent with recent resonant magnetic x-ray- and neutron-diffraction experiments,[32] which find a longer antiferromagnetic correlation length along the c^* axis in a higher-quality URu_2Si_2 single crystal. The elastic magnetic rodlike scattering above $T_N=17.5$ K may also have its origin in the stacking faults of our sample. The scattering corresponds to a finite static ferromagnetic polarization of planes perpendicular to the c^* axis, the relative orientation of the polarization of different planes being parallel or antiparallel at random. This result may be related to the weak ferromagnetic phase transition which was found by magnetization experiments in some URu_2Si_2 but shown to be absent in higher-quality samples.[33]

B. High-energy response

Whereas a large part of the low-temperature susceptibility arises from the big dipolar matrix element between the ground state and excited singlet states, the low-temperature linear specific-heat term[1] of $\gamma=50$ mJ/(mol K^2) is a signature of a continuous density of states which cannot be reconciled with the resonant responses characteristic of crystal-field systems in their ground state. As shown in Sec. III C, there are overdamped excitations above the crystal-field excitations, which presumably are responsible for the linear specific-heat term in URu_2Si_2. The characteristic energy of this response is roughly an order of magnitude above that of the overdamped response of, for example, U_2Zn_{17}.[20] The coefficient to the linear term in the specific heat, γ, of URu_2Si_2 is about an order of magnitude lower than that of U_2Zn_{17}. The characteristic energy and γ^{-1} thus roughly scale for these compounds, as expected if the magnetic neutron scattering probes the magnetic fluctuations of the heavy quasiparticles.

The high-energy response in URu_2Si_2 corresponds to a large susceptibility, $\mathrm{Im}\chi_{(1,0,0)}(2.4\ \mathrm{THz})\sim 3\times 10^{-2}$ (emu/mol unit cells) or, equivalently, $4\mu_B^2$/THz per unit cell.[15] Converting to a fluctuating moment by integration of the spectrum, we estimate the amount of moment participating in these fluctuations to be $0.6\mu_B$/(unit cell).[15] The overdamped response thus has an associated fluctuating moment smaller but comparable to that of the low-energy resonant response at (1,0,0). Also, it has the same axial anisotropy as the low-energy response. We speculate that the broad response is the signature of the hybridization of the f electrons with conduction electrons at the Fermi level. This speculation is based on the fact that the overdamped magnetic fluctuations have the same anisotropy and form factor as the sharp f spin waves, yet exhibit the continuous spectrum characteristic of conduction electrons in a metal.

Resistivity data for URu_2Si_2 further support this idea.[10] The resistivity is largest and most strongly temperature dependent in the basal plane of the tetragonal structure. This may be because a current in the basal plane is perpendicular to, and therefore scattered more strongly by, the moments which fluctuate only along the c axis. Also, it is interesting to note that the antiferromagnetic correlations build up (Fig. 14) just above the temperature at which the basal-plane resistivity passes through a maximum, followed by a low-temperature decrease by over an order of magnitude. This result is consistent with the reduction in resistivity being a consequence of the development of antiferromagnetic correlations.

V. CONCLUSIONS

The mixture of crystal-field and heavy-fermion characteristics which is found in the bulk properties of URu_2Si_2 manifests itself in the magnetic excitations at low temperatures which show a crossover between a low-energy regime of dispersive crystal-field excitations and a high-energy spectrum of overdamped antiferromagnetic fluctuations. While the presence of sharp magnetic excitations in URu_2Si_2 is unique for heavy-fermion systems, the qualitative behavior of the inelastic neutron scattering at higher-energy transfers bears some resemblance to that observed in other heavy-fermion systems.

The energies and intensities of the low-energy crystal-field excitations are well described by the singlet-singlet model, as is the direction of the ordered moment and the entirely longitudinal symmetry of the excitations. The ordered moment of $(0.04\pm0.01)\mu_B$ is, however, reduced by an order of magnitude from what this simple model predicts. It is perhaps not the primary order parameter of the phase transition at $T_N = 17.5$ K, which is accompanied more clearly by a marked decrease in the damping of low-energy magnetic fluctuations resulting in the development of a set of sharp dispersive spin waves. A small antiferromagnetic moment has also been observed in other heavy-fermion systems. In UPt_3 the ordered moment is $(0.02\pm0.01)\mu_B$ and occurs at the wave vector corresponding to the lowest-energy magnetic fluctuations.[34] It is, however, important to note that there is a gap in the low-energy excitation spectrum of URu_2Si_2, whereas this is not the case for UPt_3. Concomitantly, only in URu_2Si_2 is the development of the small ordered moment associated with an entropy change of order R. These minute ordered moments may be dependent on impurities and defects, but the absence of a larger ordered moment, despite the proximity to criticality which they imply, is an unresolved problem. It seems that the coupling between the f and conduction electrons results in a modification of the U^{4+} environment in such a way that the on-site and intersite energies scale together in the ordering of uranium-based heavy-fermion systems.

The damping of the crystal-field excitations propagating along the c^* axis and the broad spectrum of overdamped antiferromagnetic fluctuations at higher energies shows that the f-electron motion is not simply governed by interatomic correlations. The high-energy response may be thought of as the magnetic excitations of quasiparticles which have a large f electron contribution, as is experimentally shown by the longitudinal character of the excitations and the f-electron-like form factor. The itinerant nature of the quasiparticles, on the other hand, is demonstrated by the onset of a large resistivity decrease as the magnetic fluctuations of the quasiparticles become antiferromagnetically correlated.

Crystal-field effects are clearly of importance in understanding heavy-fermion systems. In URu_2Si_2 the tetragonal symmetry leads to a singlet ground state which renders what looks like a heavy-fermion system at high energies into an effective crystal-field system at low energies and temperatures. The phase transition at 17.5 K may ultimately be understood in terms of an f-electron localization which occurs in the low-energy regime. It results in crystal-field-like dynamics much like in mixed valence systems, although in the heavy-fermion case only spin degrees of freedom are involved.

ACKNOWLEDGMENTS

We thank Dr. D. Bonn and Dr. T. Timusk for allowing us to reproduce their infrared data and Dr. D. R. Taylor for useful discussions. We also thank R. L. Donaberger for technical assistance with the experiments at Chalk River. Three of us (T.E.M., M.F.C., and P.T.M.) acknowledge the financial support of the Natural Sciences and Engineering Research Council of Canada. C.B. acknowledges fruitful discussions with G. Aeppli, E. D. Isaacs, P. A. Lindgard, C. M. Varma, and A. P. Ramirez, and support from the Canadian Institute for Neutron Scattering and the Danish Research Academy during the course of the experiments at Chalk River. H.L. acknowledges support from CIDA and McMaster University.

---

*Present address: Department of Physics and Astronomy, The Johns Hopkins University, Baltimore, Maryland 21218.

†Present address: AT&T Bell Laboratories, Murray Hill, New Jersey 07974.

[1] T. T. M. Palstra, A. A. Menovsky, J. van den Berg, A. J. Dirkmaat, P. H. Kes, G. J. Nieuwenhuys, and J. A. Mydosh, Phys. Rev. Lett. **55**, 2727 (1985).

[2] M. B. Maple, J. W. Chen, Y. Dalichaouch, T. Kohara, C. Rossel, M. S. Torikachvili, M. W. McElfresh, and J. D. Thompson, Phys. Rev. Lett. **56**, 185 (1986).

[3] W. Schlabitz, J. Baumann, B. Pollit, U. Rauchschwalbe, H. M. Mayer, U. Ahlheim, and C. D. Bredl, Z. Phys. B **62**, 171 (1986).

[4] A. De Visser, F. E. Kayzel, A. A. Menovsky, J. J. M. Franse, J. van den Berg, and G. J. Nieuwenhuys, Phys. Rev. B **34**, 8168 (1986).

[5] F. R. De Boer, J. J. M. Franse, E. Louis, A. A. Menovsky, J. A. Mydosh, T. T. M. Palstra, U. Rauchschwalbe, W. Schlabitz, F. Steglich, and A. de Visser, Physica B **138**, 1 (1986).

[6] M. W. McElfresh, J. D. Thomson, J. O. Willis, M. B. Maple, T. Kohara, and M. S. Torikachvili, Phys. Rev. B **35**, 43 (1987).

[7] A. De Visser, F. R. de Boer, A. A. Menovsky, and J. J. M. Franse, Solid State Commun. **64**, 527 (1987).

[8] *Handbook on the Physics and Chemistry of Rare Earth,* edited by K. A. Gschneidner, Jr. and LeRoy Eyring (North-Holland, Amsterdam, 1979), Vols. 1 and 2.

[9] *Magnetic Properties of Rare Earth Metals,* edited by R. J. Elliot (Plenum, London, 1972).

[10] T. T. M. Palstra, A. A. Menovsky, and J. A. Mydosh, Phys. Rev. B **33**, 6527 (1986).

[11] T. E. Mason, H. Lin, M. F. Collins, W. J. L. Buyers, A. A. Menovsky, and J. A. Mydosh, Physica B **163**, 45 (1990).

[12] W. K. Kwok, L. E. DeLong, C. W. Crabtree, D. G. Hinks, and R. Joynt, Phys. Rev. B **41**, 11 649 (1990).

[13] U. Walter, C. -K. Loong, M. Loewenhaupt, and W. Schlabitz, Phys. Rev. B **33**, 7875 (1986).

[14] C. Broholm, J. K. Kjems, W. J. L. Buyers, P. Matthews, T. T. M. Palstra, A. A. Menovsky, and J. A. Mydosh, Phys. Rev. Lett. **58**, 1467 (1987).

[15] C. Broholm, Ph.D. thesis Risø-M-2731, (1989). Available by request from Risø National Laboratory, Box 49, 4000 Roskilde, Denmark.

[16] A. A. Menovsky and J. J. M. Franse, J. Cryst. Growth **65**, 286 (1983).

[17] D. C. Tennant and N. Kerley, Rev. Sci. Instrum. **60**, 136 (1988).

[18] B. C. Frazer, G. Shirane, D. E. Cox, and C. E. Olsen, Phys. Rev. **140**, A1448 (1965).

[19] H. Yoshizawa and K. Hirakawa, J. Phys. Soc. Jpn. **46**, 448 (1979).

[20] C. Broholm, J. K. Kjems, G. Aeppli, Z. Fisk, J. L. Smith, S. M. Shapiro, G. Shirane, and H. R. Ott, Phys. Rev. Lett. **58**, 917 (1987).

[21] P. A. Lindgard, in *Spin Waves and Magnetic Excitations,* edited by A. S. Borovik-Romanov and S. K. Sinha (North-Holland, Amsterdam, 1988), Vol. 22.1.

[22] G. J. Nieuwenhuys, Phys. Rev. B **35**, 5260 (1987).

[23] T. M. Holden, J. A. Jackman, W. J. L. Buyers, K. M. Hughes, M. F. Collins, P. de V. Duplessis, and O. Vogt, J. Magn. Magn. Mater. **63-64**, 155 (1987).

[24] W. J. L. Buyers, T. M. Holden, and A. Perreault, Phys. Rev. B **11**, 266 (1975); see also W. J. L. Buyers and T. M. Holden, in *Handbook of Chemistry and Physics of the Actinides,* edited by A. J. Freeman and G. H. Lander (North-Holland, Amsterdam, 1985), Vol. 2.

[25] Y. -L. Wang and B. R. Cooper, Phys. Rev. **185**, 696 (1969).

[26] J. J. M. Franse, A. A. Menovsky, A. de Visser, J. van den Berg, and G. J. Nieuwenhuys, J. Appl. Phys. **61**, 3383 (1987).

[27] U. Rauchschwalbe, Physica B **147**, 1 (1987).

[28] D. A. Bonn, J. D. Garrett, and T. Timusk, Phys. Rev. Lett. **61**, 1305 (1988).

[29] R. J. Birgeneau, in *Magnetism and Magnetic Materials,* 1972 (Denver), Proceedings of the 18th Annual Conference on Magnetism and Magnetic Maerials, AIP Conf. Proc. No. 10, edited by C. D. Graham and J. J. Rhyne (New York, 1973), p. 1664.

[30] R. W. Youngblood, G. Aeppli, and J. D. Axe, Phys. Rev. Lett. **49**, 1724 (1982).

[31] D. B. McWhan, C. Vettier, R. Youngblood, and G. Shirane, Phys. Rev. B **20**, 4612 (1979).

[32] E. D. Isaacs, D. B. McWhan, R. N. Kleiman, D. J. Bishop, G. E. Ice, P. Zschack, B. D. Gaulin, T. E. Mason, J. D. Garrett, and W. J. L. Buyers, Phys. Rev. Lett. **65**, 3185 (1990); T. E. Mason, B. D. Gaulin, J. D. Garrett, Z. Tun, W. J. L. Buyers and E. D. Isaacs, *ibid.* **65**, 3189 (1990).

[33] A. P. Ramirez, T. T. M. Palstra, T. Siegrist, J. D. Garrett, E. Bruck, A. A. Menovsky, and J. A. Mydosh (unpublished).

[34] G. Aeppli, E. Bucher, C. Broholm, J. K. Kjems, J. Baumann, and J. Hufnagl, Phys. Rev. Lett. **60**, 615 (1988).